PRAMANA
— journal of
physics

Vol. 66, No. 1
January 2006
pp. 43–54

Melting of heterogeneous vortex matter: The vortex 'nanoliquid'

S S BANERJEE[1,2,*], S GOLDBERG[2], Y MYASOEDOV[2], M RAPPAPORT[2], E ZELDOV[2], A SOIBEL[3], F DE LA CRUZ[4], C J VAN DER BEEK[5], M KONCZYKOWSKI[5], T TAMEGAI[6] and V VINOKUR[7]

[1]Department of Physics, Indian Institute of Technology Kanpur, Kanpur 208 016, India
[2]Department of Condensed Matter Physics, Weizmann Institute of Science, Rehovot 76100, Israel
[3]Jet Propulsion Laboratory, California Institute of Technology, Pasadena, California 91109, USA
[4]Instituto Balseiro and Centro Atómico Bariloche CNEA, Bariloche, 8400, Argentina
[5]Laboratoire des Solides Irradiés, CNRS UMR 7642 and CEA-DMS-DRECAM, Ecole Polytechnique, 91128 Palaiseau, France
[6]Department of Applied Physics, The University of Tokyo, Hongo, Bunkyo-ku, Tokyo 113-8656, Japan
[7]Materials Science Division, Argonne National Laboratory, Argonne, Illinois 60439, USA
[*]E-mail: satyajit@iitk.ac.in

Abstract. Disorder and porosity are parameters that strongly influence the physical behavior of materials, including their mechanical, electrical, magnetic and optical properties. Vortices in superconductors can provide important insight into the effects of disorder because their size is comparable to characteristic sizes of nanofabricated structures. Here we present experimental evidence for a novel form of vortex matter that consists of interconnected nanodroplets of vortex liquid caged in the pores of a solid vortex structure, like a liquid permeated into a nanoporous solid skeleton. Our nanoporous skeleton is formed by vortices pinned by correlated disorder created by high-energy heavy ion irradiation. By sweeping the applied magnetic field, the number of vortices in the nanodroplets is varied continuously from a few to several hundred. Upon cooling, the caged nanodroplets freeze into ordered nanocrystals through either a first-order or a continuous transition, whereas at high temperatures a uniform liquid phase is formed upon delocalization-induced melting of the solid skeleton. This new vortex nanoliquid displays unique properties and symmetries that are distinct from both solid and liquid phases.

Keywords. Inhomogeneous vortex solid; BSCCO; melting; columnar defects; magneto-optical imaging; vortex liquid.

PACS Nos 74.25.Qt; 74.25.Op; 74.25.Sv; 74.72.Hs

Porous and nanoporous materials are of significant scientific and technological interest with potential applications ranging from supercapacitors to microlasers and from medical devices to hydrogen storage [1–5]. A particle confined in a porous

matrix can be quantum mechanically treated like a particle in a box. However a larger number of interacting particles with strong particle–wall interactions makes the behavior of materials or fluids confined in a porous matrix quite complex and intractable. A novel insight into the physics of such heterogeneous systems can be gained from a porous system realized in vortices in superconductors. A unique property of the vortex matter is that the density of the vortices and the various relevant characteristic energies can be varied by orders of magnitude, which provides the possibility for investigating a wide variety of fundamental aspects of heterogeneous materials and effects of disorder.

The dynamic and thermodynamic properties of vortex matter are strongly affected by disorder and, in particular, by correlated disorder. A high concentration of correlated disorder in the form of columnar defects (CDs), for example, greatly enhances the critical current of high-temperature superconductors, which is essential for practical applications. Most of the previous studies have treated the vortex matter as a homogeneous elastic medium, which can form an ordered Abrikosov lattice in the absence of disorder, a quasi-ordered or Bragg glass phase in the presence of weak point disorder, a vortex glass in the presence of strong point disorder, or a Bose glass in the presence of CDs [6–17]. Recently, however, it has been shown that a new 'porous' vortex solid can be formed in the presence of a low density of CDs [18,19]. In this configuration two distinct intercalated sub-systems of vortices are formed: vortices residing on CDs are strongly pinned and create a rigid porous skeleton, while the interstitial vortices form relatively ordered nanocrystals intercalated within the voids of this porous skeleton. This experimental finding has stimulated a series of theoretical studies and numerical simulations [20–26]. In this paper, we describe the existence of a new 'nanoliquid' phase that is found in-between the porous solid and the homogeneous liquid phases in the field (B)–temperature (T) diagram [27]. One of the interesting properties of this novel phase is that the dissipationless superconductivity perpendicular to the magnetic field is lost, while a phase coherence along the direction of the vortices is apparently preserved.

We have created CDs in $Bi_2Sr_2CaCu_2O_8$ (BSCCO) single crystals ($T_c \approx 90$ K) using low irradiation doses of 1 GeV Pb ions at GANIL, France. Figure 1d shows the locations of the CDs revealed by etching mica that was irradiated simultaneously with the crystals and imaged using an AFM. The CDs form a dense network or matrix that contains numerous voids that are free of columns. Two such voids, or pores, are outlined schematically by the light color in figure 1d. This seemingly inhomogeneous distribution of CDs is in fact consistent with Poisson statistics of random ion irradiation. The CDs act as strong pinning centers for the vortices and therefore at low magnetic fields all the vortices reside on CDs. When the field approaches the matching field $B_\phi = n\Phi_0$, where n is the aerial density of CDs and Φ_0 is the flux quantum, most of the CDs become occupied by vortices [28]. This network of rigid vortices is the skeleton of the porous vortex matter. Upon further increase of the magnetic field B, the extra vortices form ordered nanocrystals within the pores of the skeleton. Our recent low temperature Bitter magnetic decoration studies [18,19] have shown that the physical size of the voids remains fixed, while the number of vortices in the voids increases linearly with B. As a result we can readily change the number of vortices in the nanocrystals from a few vortices to

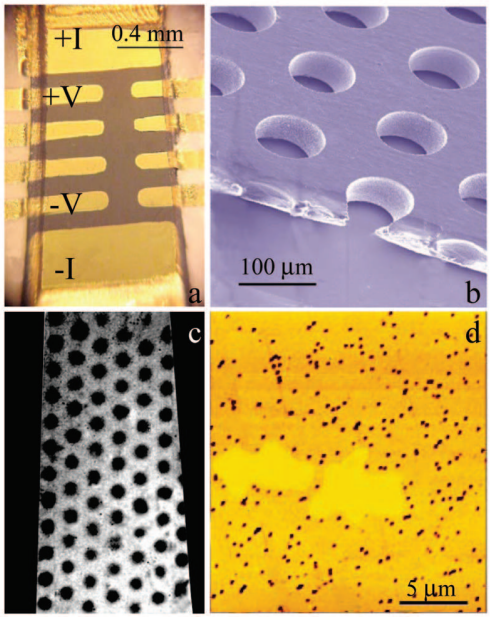

Figure 1. Sample geometry and irradiation procedure. (**a**) Image of the BSCCO crystal of dimensions $1.5 \times 0.8 \times 0.025$ mm^3 with 50 nm thick evaporated gold strips. The strips extend onto the sapphire substrate and current and voltage contacts are wire-bonded to the strips. (**b**) SEM image of the stainless steel mask that covers the sample during the 1 GeV Pb irradiation, resulting in the formation of columnar defects only within the 90 μm diameter apertures. (**c**) Differential magneto-optical image of the crystal obtained with a field modulation of 1 G at $B = 45$ G and $T = 79$ K. The dark spots show strong vortex pinning in the irradiated regions ($B_\phi = 60$ G), whereas the pristine areas remain reversible. The regions outside the sample have been artificially darkened. (**d**) A 20×20 μm^2 AFM image of an etched piece of mica irradiated along with the BSCCO crystals ($B_\phi = 20$ G). The dark spots reveal the locations of the columnar defects while the regions colored in bright yellow are examples of two of the voids in the distribution of columns.

hundreds of vortices by simply varying the applied field. As shown, these variable size nanocrystals melt into vortex nanodroplets confined within the voids. In the absence of CDs, the vortex matter undergoes a single first-order melting transition into a homogeneous liquid when thermal energy becomes comparable to the elastic energy of the lattice [29–33]. In contrast, we find here two separate transitions defining a Y-shaped phase boundary of a new nanoliquid phase squeezed in-between the porous solid and the homogeneous vortex liquid phase.

For this study we have used a combination of several experimental techniques on specially designed samples, as seen in figure 1. Figure 1a shows one of the BSCCO crystals glued to a sapphire substrate onto which gold contacts were evaporated to allow simultaneous transport and magneto-optical imaging investigations. The gold strips connect the top surface of the crystal to electrical pads on the sapphire

substrate. The pads are a few millimeters away from the crystal in order to allow placing a magneto-optical indicator film onto the crystal without interfering with the electrical wiring. The samples were covered with a 50 μm thick stainless steel mask with an array of 90 μm diameter apertures shown in figure 1b. The crystals were subsequently irradiated with 1 GeV Pb ions. The mask blocks the ions and as a result CDs are formed in BSCCO crystals only within the 90 μm apertures. The AFM image in figure 1d shows a typical distribution of CDs within the irradiated apertures for an irradiation dose corresponding to $B_\phi = 20$ G. As described below the advantage of using the mask is that differences in vortex matter properties in irradiated and pristine regions in the same crystal can be resolved with high sensitivity and precision. For example, figure 1c shows the difference in the shielding of magnetic field between the irradiated regions (array of dark circular regions) and the pristine regions (gray areas) obtained by differential magneto-optical (DMO) imaging with field modulation, as described below.

In order to determine the existence of possible different vortex matter phases, there is a need for experimental techniques that can distinguish between solid and liquid states, and in addition, in our case, between different possible liquid phases. We have therefore used four different experimental methods. To distinguish between solids and liquids, field modulation and temperature modulation DMO imaging techniques were employed [18,34–37]. However, the determination of different liquid phases is experimentally more challenging and cannot be addressed by these methods. For this purpose we have developed a new, very sensitive technique for the visualization of transport current flow and have combined it with resistive measurements.

We first determine the location of the solid–liquid transition in our samples. In clean BSCCO crystals the melting occurs through a first-order transition (FOT) that can be directly visualized using DMO imaging [34–37]. Figure 2a shows the nucleation of the liquid phase in the central part of the crystal obtained by DMO with temperature modulation. The dark blue areas show the location of the liquid phase and the orange areas show the location of the vortex solid phase at $T = 78.7$ K. By periodically modulating the temperature by 0.3 K the liquid regions expand and contract. Similar to water, the vortex density in the liquid, n_l, is higher than that in the solid, n_s, and therefore in the regions to which the liquid expands within the temperature modulation the local induction B increases by $\Delta B = (n_\mathrm{l} - n_\mathrm{s})\Phi_0$. These regions are seen in light blue color at the interface with the solid regions (brown). This light paramagnetic signal is the thermodynamic signature [38] of the FOT. ΔB is of the order of 0.1 G and therefore requires sensitive differential imaging and extensive integration to be visualized. The interesting feature in figure 2a is that the vortex lattice melts in the pristine regions while the irradiated apertures remain solid (dark brown). Figure 2b shows that the irradiated regions start to melt at substantially higher temperatures while strikingly preserving the first-order nature of the transition (cyan).

Figures 3a and 3b show the location of the melting transition on the B–T phase diagram in the pristine, $B_\mathrm{m}^0(T)$, and in the irradiated, $B_\mathrm{m}^\mathrm{CD}(T)$, regions for samples with $B_\phi = 60$ G and 20 G respectively. With decreasing temperature along the $B_\mathrm{m}^\mathrm{CD}(T)$ line the strength of the FOT in the irradiated regions diminishes, becoming weakly first-order and eventually turning apparently into a second-order transition

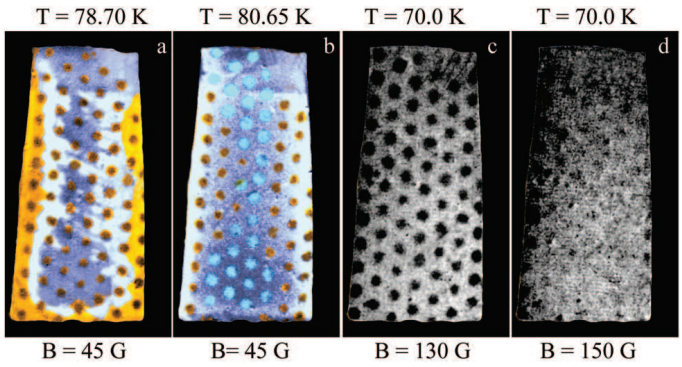

Figure 2. Differential magneto-optical images of the vortex lattice melting process and images of the transformation from the irreversible to the reversible response of the vortex matter in the BSCCO crystal of figure 1 irradiated through the mask. The differential images in (a) and (b) were obtained using temperature modulation of 0.3 K at $B = 45$ G. (**a**) Melting in the pristine parts of the sample. Color code: orange denotes vortex solid in the pristine regions, brown – vortex solid in the irradiated circular regions ($B_\phi = 60$ G), and dark blue – vortex liquid phase in the pristine regions. The light blue signal shows the regions that periodically undergo the first-order melting transition in response to the 0.3 K temperature modulation. (**b**) All the pristine regions of the sample are in the liquid phase, while some of the irradiated regions are solid (brown) and others are liquid (cyan). The differential images in (**c**) and (**d**) were obtained using field modulation of 1 G at $T = 70$ K and $B = 130$ G and 150 G respectively. The gray regions show a reversible response to field modulation while the dark circles are the irradiated irreversible regions of the sample that shield the AC field. The regions outside the sample have been artificially darkened.

[18,39]. Thus in order to map out the full $B_{\rm m}^{\rm CD}(T)$ line at lower temperatures, we use DMO with field modulation instead of temperature modulation which enables us to distinguish between the reversible and irreversible regions of the sample. Figure 2c shows a DMO image of the central part of the crystal (for $B_\phi = 60$ G) using field modulation of 1 G at $T = 70$ K and $B = 130$ G, which is in-between $B_{\rm m}^{0}(T)$ and $B_{\rm m}^{\rm CD}(T)$ lines in figure 3a. In this situation all the pristine regions of the sample have already melted and are visible in gray showing that the field modulation fully penetrates these reversible liquid regions. The irradiated apertures appear dark since they are still in the solid phase below $B_{\rm m}^{\rm CD}(T)$ and hence the field modulation is shielded due to vortex pinning. At $B_{\rm m}^{\rm CD}(T)$ the irradiated apertures melt and the entire sample becomes reversible as seen in figure 2d. The open circles in figure 3 were obtained using field modulation while the solid circles using temperature modulation.

We now search for a possible new liquid–liquid transition between different liquid phases. Such a possible transition has been considered recently [18,20,23] but has not been found experimentally. Since we do not expect this liquid–liquid transition to be strongly first-order and since the liquid phases are reversible, the two DMO methods described above cannot resolve this transition. We have therefore

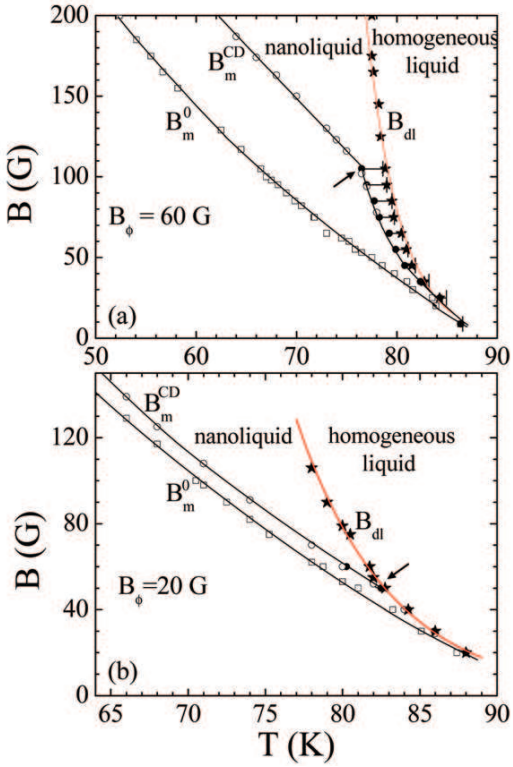

Figure 3. B–T vortex matter phase diagram showing the nanoliquid phase. (**a**) $B_{\rm m}^0(T)$ is the vortex lattice melting line in the pristine regions and $B_{\rm m}^{\rm CD}(T)$ is the melting line in the irradiated regions with $B_\phi = 60$ G. The $B_{\rm dl}(T)$ delocalization line separates the vortex nanoliquid from the homogeneous liquid phase. The black lines are guides to the eye and the red $B_{\rm dl}(T)$ line is the best fit to the theoretically predicted exponential form $\exp(-T/T_0)$, see text. The arrow indicates the location of the kink in the $B_{\rm m}^{\rm CD}(T)$ line. (**b**) A similar phase diagram for a sample irradiated with $B_\phi = 20$ G.

developed a new differential technique. Instead of modulating the applied field or temperature, a transport current with periodically modulated polarity is applied to the sample and a corresponding differential image is acquired and integrated, typically over a hundred cycles. As a result, the self-induced magnetic field generated by the transport current according to the Biot–Savart law can be measured to very high precision. With this differential imaging we are able to determine the distribution of currents as low as 0.1 mA. Conventional MO has been used previously to map the current flow in superconductor films and tapes usually using pulsed currents of few Amps [40–43]. Our differential method thus presents more than three orders of magnitude improvement in sensitivity.

Figure 4a shows the self-induced magnetic field in the central part of the sample resulting from 50 mA transport current. This image displays the behavior at $T =$ 74.2 K and $B = 145$ G, which is above the $B_{\rm m}^{\rm CD}(T)$ line, namely the entire sample

is in the liquid phase. Surprisingly, despite the fact that both the irradiated and pristine regions are liquid, strong variations in the self-induced field are found as shown in figure 4b, indicating a highly inhomogeneous current distribution. Using the matrix inversion technique [44–46] of the Biot–Savart law, a direct measure of the flow behavior of the transport current is obtained as shown in figures 4c and 4d. The current is strongly focused into the irradiated regions reaching densities up to seven times higher than in the unirradiated regions. This means that the vortex liquid phase in the irradiated regions has a much lower resistivity and the vortices experience a much higher effective viscosity as compared to the pristine liquid phase. Figures 4b and 4d also show the evolution of the self-field and current distribution with increasing temperature. At 79 K the current distribution becomes uniform quite abruptly and remains uniform at higher temperatures, indicating that above this temperature the two liquid phases become identical. As described below, we identify this temperature as the delocalization temperature $T_{\rm dl}$ separating the nanoliquid phase from a homogeneous liquid phase. Figure 3 shows the location of this nanoliquid delocalization line $B_{\rm dl}(T)$ on the phase diagram.

We have also performed transport measurements simultaneously with DMO imaging. Figure 5a shows the measured four-probe resistance R of the sample as a function of temperature at various fields. The arrows indicate the delocalization temperature $T_{\rm dl}$ as derived from the DMO self-field measurements. A clear kink and a rapid decrease in the resistance are visible below this temperature, consistent with the decrease in the resistance in the irradiated regions deduced from the DMO self-field data. Note that in BSCCO crystals the transport data is usually available only above $B^0_{\rm m}(T)$, while below $B^0_{\rm m}(T)$ the sample is in the solid phase where the resistance is often too low to be measured. In BSCCO crystals, the resistance in the liquid phase has Arrhenius behavior [47,48] as seen in figure 5b. In our special geometry we should expect the following behavior. In the homogenous liquid region, R should decrease smoothly with decreasing temperature until $T_{\rm dl}$ is reached, followed by a rapid drop due to the suppression of the resistance of the nanoliquid in the irradiated regions. Note, however, that the volume of the irradiated regions is only about half the total volume of the sample. Therefore, even if the resistance of the irradiated regions should become vanishingly small, the total measured R of the sample should drop approximately by a factor of two since the pristine regions, occupying about half of the sample, remain liquid down to $T^0_{\rm m}$ in figure 5b and maintain the usual highly resistive Arrhenius behavior. Such a drop between two parallel Arrhenius lines is indeed observed and is emphasized by the dotted lines in figure 5b. However, the striking observation is that the drop is by a factor of 20 or more instead of a factor of two. This behavior shows that the c-axis correlation of the caged nanoliquid is significantly higher than that of the homogeneous liquid, for the following reason. Because of the high anisotropy of BSCCO the applied current flows in a very shallow layer underneath the top surface of the crystal where the electrical contacts are attached [49–51]. The characteristic depth of the current is inversely proportional to the effective anisotropy $\gamma_\rho = (\rho_c/\rho_{ab})^{1/2}$, where ρ_c and ρ_{ab} are the c-axis and in-plane resistivities. In BSCCO crystals $\gamma_\rho \approx 500$ and may change considerably depending on oxygen doping and temperature. The enhanced c-axis correlation of the nanoliquid significantly reduces ρ_c and the anisotropy in the irradiated regions. As a result, the irradiated regions allow the current to

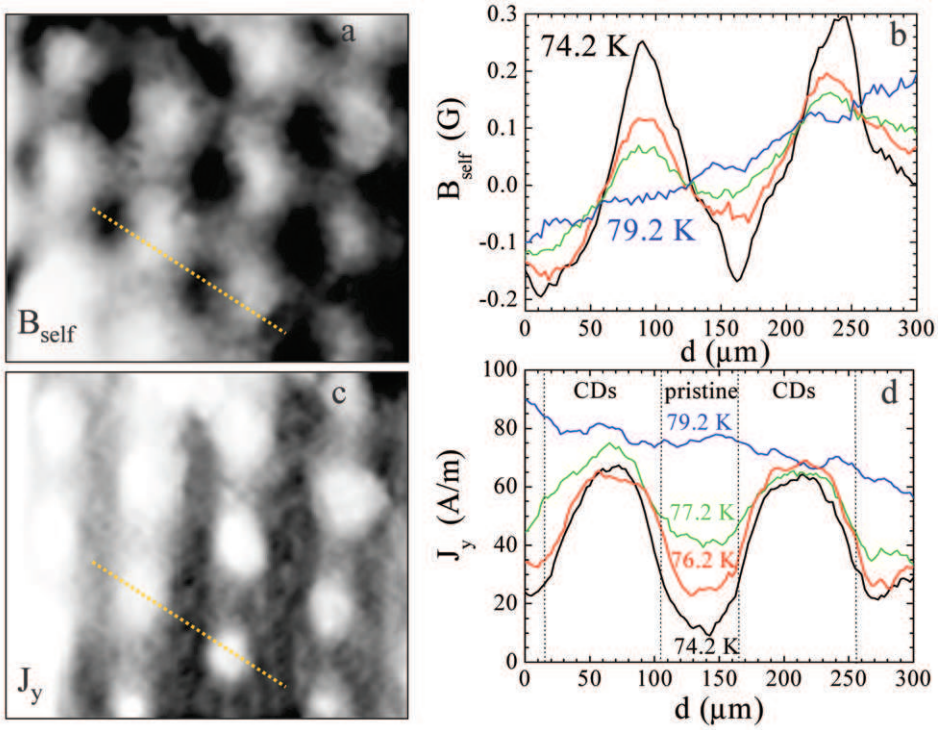

Figure 4. Transport current flow patterns in nanoliquid phase in irradiated regions. (**a**) Differential magneto-optical image of the transport current self-induced magnetic field in the central part of the sample at $B = 145$ G and $T = 74.2$ K. The image is obtained by periodically subtracting an image taken with -50 mA applied current from that with $+50$ mA and averaging over a large number of periods. The bright and dark shades correspond to positive and negative values of self-induced magnetic field. (**b**) Profiles of the self-field along the yellow dashed line in (a) at different temperatures. (**c**) Current distribution obtained by inversion of the self-field image in (a). (**d**) Profiles of the current density distribution along the yellow line in (c) at different temperatures with indicated irradiated and pristine regions. Even though the temperature is well above the melting temperature in all the regions, the current density in the irradiated regions ($B_\phi = 60$ G) is significantly higher, showing that the resistance in the nanoliquid phase is much lower than in the homogeneous liquid. The current flow becomes uniform above the delocalization temperature as shown by the 79.2 K curve.

penetrate deeper into the crystal, thereby increasing the effective thickness of the sample. Since the resistance of the sample drops by a factor of more than twenty, we conclude that the nanoliquid is at least an order of magnitude more isotropic than the homogenous liquid.

We now discuss the phase boundaries in figure 3 from the symmetry breaking standpoint. There are two symmetries that are broken upon freezing into the

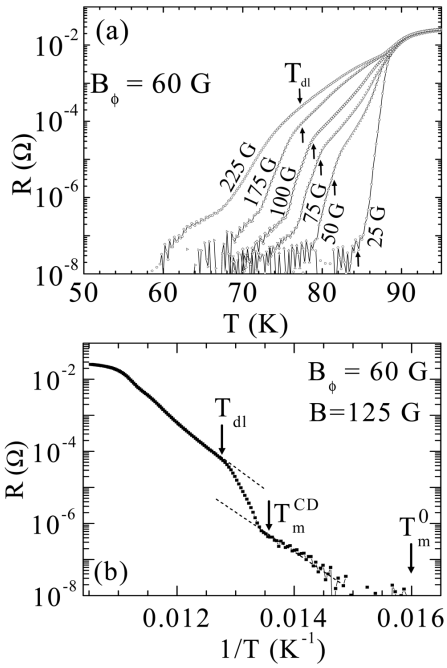

Figure 5. (**a**) Sample resistance vs. temperature at various fields. The delocalization temperatures $T_{\rm dl}$, denoting the transition from the nanoliquid to the homogenous liquid phase as derived from DMO self-field data, are marked by the arrows. (**b**) Example of Arrhenius plot of $R(T)$ at $B = 125$ G emphasizing the step-like drop in the resistance below $T_{\rm dl}$. The melting temperatures in the presence of CDs and in the pristine case as derived by DMO viz., $T_{\rm m}^{\rm CD}$ and $T_{\rm m}^{0}$, at 125 G are marked for comparison.

vortex solid phase [6]: the formation of the Abrikosov lattice within the nanocrystals breaks the continuous translational symmetry of the vortex liquid, and the appearance of the supercarrier density and the resulting ability to sustain dissipationless currents along the vortices breaks the longitudinal gauge symmetry. Note that the translational order within the nanocrystals is preserved to elevated temperatures by the caging potential of the porous skeleton that suppresses the lateral thermal fluctuations of the vortices. Thus, the melting line $B_{\rm m}^{\rm CD}(T)$ above the kink is shifted upwards significantly as compared to the pristine melting line $B_{\rm m}^{0}(T)$. At $B_{\rm m}^{\rm CD}(T)$ the nanocrystals melt into nanodroplets, restoring the transverse translational symmetry. The rigid skeleton, however, remains intact due to the strong pinning by the CDs, thus preserving the longitudinal c-axis correlation along the CDs up to the $B_{\rm dl}(T)$ line. The resulting nanoliquid phase, consisting of interconnected nanodroplets caged in a porous skeleton, has a unique property of extended c-axis coherence together with the absence of in-plane critical current, suggesting that in our case the two symmetries involved are broken sequentially. Several recent theoretical studies and numerical simulations [20,23,25] indeed find evidence for superconducting coherence along the c-axis in the intermediate liquid

phase. More specifically, using the analogy between vortices and two-dimensional bosons [6,13], an intermediate superfluid state in which the superfluid condensate of bosons (vortex liquid) coexists with localized bosons (vortices pinned on CDs) has been predicted [23,24]. With increasing temperature the intermediate vortex liquid system (nanoliquid) undergoes a sharp delocalization crossover above which all the vortices become delocalized (homogeneous liquid), thereby rendering the system incapable of sustaining any supercurrents along the vortices. The delocalization line follows an exponential temperature dependence, $B_{\rm dl}(T) \propto \exp(-T/T_0)$, with estimated [23] $T_0 \sim 5$ K for typical parameters of BSCCO. The red lines in figure 3 are exponential fits to the data resulting in $T_0 \approx 7.7$ K for the $B_\phi = 60$ G sample (figure 3a) and $T_0 \approx 13.9$ K for the $B_\phi = 20$ G crystal (figure 3b) which had a slightly higher $T_{\rm c}$. We have also studied a crystal with $B_\phi = 47$ G (not shown) resulting in $T_0 \approx 7.3$ K. In all three cases the theoretical temperature dependence provides a very good description of the experimental $B_{\rm dl}(T)$ line. Note, however, that the theory does not take into account the discreteness associated with the vortex pancakes and therefore its applicability to BSCCO should be further investigated. Alternative estimate, based on Berezinskii–Kosterlitz–Thouless-like scenario of delocalization of the two-dimensional pancake vortices [14], also yields an exponential temperature dependence of $B_{\rm dl}(T)$ with proper parameters. Thus, we surmise that the longitudinal gauge symmetry that is broken in the nanoliquid is restored above the $B_{\rm dl}(T)$ line. It is commonly believed that the formation of the solid vortex lattice causes simultaneous breaking of the two symmetries across the FOT. Our findings here show the first phase diagram identifying two separate phase boundaries $B_{\rm m}^{\rm CD}(T)$ and $B_{\rm dl}(T)$ across which the two symmetries of the vortex matter are apparently broken separately. This unique property is the result of heterogeneous nature of the vortex nanoliquid.

It is interesting to note that the two phase boundaries $B_{\rm m}^{\rm CD}(T)$ and $B_{\rm dl}(T)$ intersect at a kink marked by arrows in figure 3. At fields below the kink the two symmetries are apparently broken simultaneously, where the $B_{\rm m}^{\rm CD}(T)$ line closely follows the delocalization line $B_{\rm dl}(T)$. Here the nanocrystals are only few vortices in size and therefore remain solid all the way to $B_{\rm dl}(T)$ due to the strong caging potential that suppresses thermal fluctuations. The delocalization of the skeleton at $B_{\rm dl}(T)$ destroys the cages resulting in restoration of the large thermal fluctuations and hence in the instantaneous melting of the entire lattice. This is a novel kind of vortex lattice melting in which delocalization [14,23] of one sub-system of vortices induces a FOT in the entire heterogeneous system. Note that the finite distribution of the nanocrystal sizes results in broadening of the FOT, as indicated by the error bars in figure 3a. The FOT apparently commences upon melting of the regions with larger crystallites while the global homogeneous liquid is established only upon melting of the smallest of the crystallites. Interestingly, this broadening is hardly resolvable for lower irradiation doses as seen in figure 3b.

In conclusion, we have found evidence for a new form of vortex matter in which nanodroplets of vortex liquid coexist with a porous skeleton of vortices localized by columnar defects. This nanoliquid or interstitial phase is formed when the vortex density exceeds the density of columnar defects. We find two separate transitions forming a Y-shaped phase diagram with the nanoliquid phase located between porous solid and homogeneous liquid phases. The nanoliquid has zero critical

current like the homogeneous vortex liquid, but the c-axis correlation and the vortex viscosity are similar to the vortex solid phase. The skeleton induces a high degree of alignment along the vortex pancake stacks resulting in very low c-axis resistivity and low anisotropy. In the presence of a driving force the vortices flow through nanoscale channels in the pinned vortex skeleton and hence experience a high shear viscosity similar to vortex flow in microfabricated structures [52–54]. Since the density of the vortices in the nanodroplets can be varied continuously, this new system can provide important insight into the thermodynamics and the flow dynamics in nanoporous materials hosting various liquid and gaseous substances [55,56]. We conjecture that the nanoliquid phase with coexisting localized and delocalized particles may be generic to strongly interacting systems in the presence of disorder.

Acknowledgments

We thank M Menghini, Y Fasano, E H Brandt and V Geshkenbein for stimulating discussions and R J Wijngaarden for providing the matrix inversion algorithm. This work was supported by the Israel Science Foundation Center of Excellence, by the German–Israeli Foundation G.I.F., and by the Minerva Foundation, Germany. The work of FdlC was partially supported by Fundacion Antorchas and by ANPCYT PICT99-5117, and of VV by the US Department of Energy, Office of Science. TT acknowledges the support of the Grant-in-Aid for Scientific Research from the Ministry of Education, Culture, Sports, Science and Technology, Japan. EZ acknowledges the support by the US–Israel Binational Science Foundation (BSF) and by the Wolfson Foundation.

References

[1] M E Davis, *Nature* **417**, 813 (2002)
[2] P Yang *et al*, *Science* **287**, 465 (2000)
[3] Y Gogotsi *et al*, *Nature Materials* **2**, 591 (2003)
[4] L N Rosi *et al*, *Science* **300**, 1127 (2003)
[5] D Maspoch *et al*, *Nature Materials* **2**, 190 (2003)
[6] G Blatter *et al*, *Rev. Mod. Phys.* **66**, 1125 (1994)
[7] E H Brandt, *Rep. Prog. Phys.* **58**, 1465 (1995)
[8] T Nattermann and S Scheidl, *Adv. Phys.* **49**, 607 (2000)
[9] T Giamarchi and P Le Doussal, *Phys. Rev.* **B52**, 1242 (1995)
[10] T Klein *et al*, *Nature* **413**, 404 (2001)
[11] A Petrean *et al*, *Phys. Rev. Lett.* **84**, 5852 (2000)
[12] U Divakar *et al*, *Phys. Rev. Lett.* **92**, 237004 (2004)
[13] D R Nelson and V M Vinokur, *Phys. Rev. Lett.* **68**, 2398 (1992)
[14] C J Van der Beek *et al*, *Phys. Rev. Lett.* **86**, 5136 (2001)
[15] S A Grigera *et al*, *Phys. Rev. Lett.* **81**, 2348 (1998)
[16] L Radzihovsky, *Phys. Rev. Lett.* **74**, 4923 (1993)
[17] P Sen *et al*, *Phys. Rev. Lett.* **86**, 4092 (2001)
[18] S S Banerjee, *Phys. Rev. Lett.* **90**, 087004 (2003)

[19] M Menghini *et al*, *Phys. Rev. Lett.* **90**, 147001 (2003)
[20] Y Nonomura and H Xiao, *Euro. Phys. Lett.* **65**, 533 (2004)
[21] C Dasgupta and O T Valls, *Phys. Rev. Lett.* **91**, 127002 (2003)
C Dasgupta and O T Valls, *Phys. Rev.* **B69**, 214520 (2004)
[22] S Tyagi and Yadin Y Goldschmidt, *Phys. Rev.* **B67**, 214501 (2003)
[23] A V Lopatin and V M Vinokur, *Phys. Rev. Lett.* **92**, 067008 (2004)
[24] J Kierfeld and V M Vinokur, *Phys. Rev. Lett.* **94**, 077005 (2005)
[25] J P Rodriguez, *Phys. Rev.* **B70**, 224507 (2004)
[26] A Morozov *et al*, *Phys. Rev.* **B67**, 140505 (2003)
[27] S S Banerjee *et al*, *Phys. Rev. Lett.* **93**, 097002 (2004)
[28] H Dai *et al*, *Science* **265**, 1552 (1994)
[29] H Safar *et al*, *Phys. Rev. Lett.* **69**, 824 (1992)
[30] W K Kwok *et al*, *Phys. Rev. Lett.* **69**, 3370 (1992)
[31] H Pastoriza *et al*, *Phys. Rev. Lett.* **72**, 2951 (1994)
[32] E Zeldov *et al*, *Nature* **375**, 373 (1995)
[33] A Schilling *et al*, *Nature* **382**, 791 (1996)
[34] A Soibel *et al*, *Nature* **406**, 282 (2000)
[35] A Soibel *et al*, *Phys. Rev. Lett.* **87**, 167001 (2001)
[36] M Yasugaki *et al*, *Phys. Rev.* **B65**, 212502 (2002)
[37] C J van der Beek *et al*, *Proceedings of the NATO Advanced Research Workshop on Magneto-Optical Imaging Oystese*, Norway, edited by T H Johansen and D V Shantsev, August 27–31, 2003 (Kluwer) pp. 79
[38] N Morozov *et al*, *Phys. Rev.* **B54**, R3784 (1996))
[39] B Khaykovich *et al*, *Phys. Rev.* **B57**, R14088 (1998)
[40] M V Indenbom *et al*, *J. Alloys and Compounds* **195**, 499 (1993)
[41] U Welp *et al*, *Nature* **376**, 44 (1995)
[42] M E Gaevski *et al*, *Phys. Rev.* **B59**, 9655 (1999)
[43] D Larbalestier *et al*, *Nature* **414**, 368 (2001)
[44] R J Wijngaarden *et al*, *Phys. Rev.* **B54**, 6742 (1996)
[45] R J Wijngaarden *et al*, *Physica* **C295**, 177 (1998)
[46] E H Brandt, *Phys. Rev.* **B46**, 8628 (1992)
[47] T T M Palstra *et al*, *Phys. Rev. Lett.* **61**, 1662 (1988)
[48] D T Fuchs *et al*, *Phys. Rev. Lett.* **81**, 3944 (1998)
[49] R Busch *et al*, *Phys. Rev. Lett.* **69**, 522 (1992)
[50] H Safar *et al*, *Phys. Rev.* **B46**, 14238 (1992)
[51] B Khaykovich *et al*, *Phys. Rev.* **B61**, R9261 (2000)
[52] N Kohubo *et al*, *Phys. Rev. Lett.* **88**, 247004 (2002)
[53] C M Marchetti and D Nelson, *Physica* **C330**, 105 (2000)
[54] C J Olson *et al*, *Phys. Rev. Lett.* **87**, 177002 (2001)
[55] J S Andrade *et al*, *Phys. Rev. Lett.* **79**, 3901 (1997)
[56] C C Lundstrom *et al*, *Science* **270**, 1958 (1995)